

RSC Advances



This is an *Accepted Manuscript*, which has been through the Royal Society of Chemistry peer review process and has been accepted for publication.

Accepted Manuscripts are published online shortly after acceptance, before technical editing, formatting and proof reading. Using this free service, authors can make their results available to the community, in citable form, before we publish the edited article. This *Accepted Manuscript* will be replaced by the edited, formatted and paginated article as soon as this is available.

You can find more information about *Accepted Manuscripts* in the [Information for Authors](#).

Please note that technical editing may introduce minor changes to the text and/or graphics, which may alter content. The journal's standard [Terms & Conditions](#) and the [Ethical guidelines](#) still apply. In no event shall the Royal Society of Chemistry be held responsible for any errors or omissions in this *Accepted Manuscript* or any consequences arising from the use of any information it contains.



ARTICLE

Enhanced corrosion performance of Zn coating by incorporating graphene oxide electrodeposited from deep eutectic solvent

Received 00th January 20xx,
Accepted 00th January 20xx

Ruiqian Li,^{a, b} Jun Liang,^{a*} Yuanyuan Hou,^{a, b} and Qingwei Chu^{a, b}

DOI: 10.1039/x0xx00000x

www.rsc.org/

In this work, a novel zinc-graphene oxide (Zn-GO) composite coatings were successfully prepared by pulse electrodeposition in choline chloride (ChCl)/urea based deep eutectic solvent (DES). The GO sheets exhibited excellent dispersion stability in ChCl:2urea DES without stabilizing additives and were uniformly deposited in the Zn matrix. The surface morphology and texture structure of Zn-GO composite coatings were quite different from those of pure Zn coating, owing to the effects of GO on the electrochemical deposition behavior of Zn(II). The Zn-GO composite coatings showed higher stability and better corrosion resistance than the pure Zn coating and the corrosion resistance of Zn-GO composite coatings increased with the increment of the GO concentration.

1. Introduction

Zinc coatings are widely used to prevent the corrosion of many metals through providing the barrier protection and/or the sacrificial protection. However, the corrosion resistance of pure Zn coating is not satisfactory under severe working conditions. Metal matrix composite coatings (MMCs) are getting more and more attention owing to their better performance than pure metal coatings due to the introduction of the reinforcements. The methods that have been used to fabricate the MMCs include physical vapor deposition (PVD), chemical vapor deposition (CVD), electroless plating, electrodeposition and powder metallurgy, and so on. Among them, electrodeposition is one of the most effective and economic methods. At present, many Zn-matrix composite coatings with different reinforcements,

such as Zn-TiO₂,¹ Zn-SiO₂,² Zn-CeO₂,³ Zn-CNT,⁴ Zn-SiC,⁵ Zn-graphene⁶ and Zn-halloysite nanotubes⁷ have been prepared by the electrodeposition process. All these Zn matrix composite coatings showed superior corrosion resistance than the pure Zn coating.

Graphene, a two dimensional one atom thick sheet with sp² hybridized carbon structure, has been attracted comprehensive attention due to its unique properties such as excellent chemical inertness, high mechanical strength, high optical transparency, good thermal and chemical stability, high electrical conductivity and exceptional impermeability to ion diffusion.^{8, 9} However, graphene is difficult to disperse in either aqueous or non-aqueous solvents, which limited the wide use in many fields. On the other hand, graphene oxide (GO), which is the most common chemically modified graphene with carboxyl and carbonyl functional groups on their edges and epoxide and hydroxyl functional groups on their basal plane,¹⁰ is hydrophilic and readily dispersible in aqueous and organic solvents.^{11, 12} Owing to the excellent dispersion stability and similar properties to graphene, GO has been used in biomedical

^a State Key Laboratory of Solid Lubrication, Lanzhou Institute of Chemical Physics, Chinese Academy of Sciences, Lanzhou 730000, People's Republic of China. E-mail: jliang@licp.cas.cn.

^b University of Chinese Academy of Sciences, Beijing 100049, People's Republic of China

devices,¹³ solid phase microextraction,¹⁴ biosensors and electrochemical sensors,¹⁵ drug delivery,¹⁶ cellular image¹⁷ and corrosion resistant coatings.¹⁸

Hitherto different coating systems related with the GO such as pure GO coating, functionalized GO coatings and GO-polymer composite coatings have been already proven to show excellent corrosion resistance. He et al.¹⁹ have demonstrated that homogeneous and dense GO coatings produced by electrophoretic deposition (EPD) can be treated more efficiently as a corrosion inhibitor to protect NdFeB from NaCl aqueous solution. Marimuthu et al.²⁰ reported that the sodium functionalized graphene oxide (NaGO) coating increased the corrosion resistance of titanium based ortho-implants as a geometric blocking layer. Compared to pure GO coatings, the NaGO coatings have a better corrosion resistance due to the formation of an intense and stable NaGO layer on titanium substrate. Krishnamoorthy et al.²¹ developed a multifunctional graphene nanopaint by mixing GO sheets and alkyd resin. The nanopaint exhibited excellent corrosion resistance, antibacterial and antifouling properties in both high salt content and acidic solutions. Singh et al.⁹ investigated the oxidation resistance and corrosion resistance of graphene oxide-polymer composite (GOPC) coating by EPD and found that the GOPC coatings has an superior oxidation resistance and corrosion resistance properties under severe chlorine ion environment.

To the best of our knowledge, however, there has been no effort to use GO as a reinforcement to fabricate corrosion resistant metal matrix composite coating. In this work, the electrodeposition of Zn-GO composite coatings on copper substrate was carried out in ChCl:2urea deep eutectic solvent (DES) and the effects of GO on the nucleation/growth process, the microstructure and the corrosion performance of Zn coating were investigated. Using DES as the electrolyte in this work is mainly based on the following points. First of all, as a new type of ionic liquid, DES has shown promising potentials in electrodeposition of metals, alloys and composites due to its excellent properties, such as wide potential windows, high ionic conductivity, high solubility of metal salts and high viscosity.²² The

reinforcements which have been studied in the DES include Al_2O_3 ,²³ SiC ,²⁴ Si_3N_4 ,²⁵ PTFE²⁶ and CNT²⁷ etc. The DES provides excellent dispersion stability of particles due to its high viscosity and ionic strength, which can overcome the shortcomings in aqueous solution, viz. poor dispersion stability of the reinforcements in plating bath and low content of the particulates in matrix metals. Secondly, our investigations showed that the GO particles can be stably suspended in the DES with the presence of metal ions. However, quickly settling down of the GO particles was observed in aqueous solution containing metal ions without stabilizing additives.

2. Experimental

2.1 Preparation of GO dispersed deep eutectic solvent

Choline chloride [$\text{HOC}_2\text{H}_4\text{N}(\text{CH}_3)_3\text{Cl}$] (ChCl, AR, $\geq 99\%$), urea [CON_2H_4] (AR, $\geq 99\%$) and zinc chloride [ZnCl_2] (AR, $\geq 99\%$) were used as received. The deep eutectic solvent (DES) was prepared by stirring the ChCl and urea in a molar ratio of 1:2 at 70 °C until a homogeneous colourless liquid was formed. Then the appropriate amount of ZnCl_2 powder was added to the DES with gentle stirring to obtain 0.2 molar ZnCl_2 per litre of DES (i.e. 0.2 M ZnCl_2) colourless transparent liquid (denoted as “pure Zn” in the following sections). GO sheets, which were prepared by oxidizing natural graphite powder using a method similar to the Hummer’s approach,²⁸ were added into the solution and stirred by a magnetic stirrer for 24 h. The concentration of GO in the DES was 0.05 g L⁻¹ and 0.10 g L⁻¹, respectively (denoted as “Zn-0.05GO” and “Zn-0.10GO”, respectively).

2.2 Electrochemical tests

All the electrochemical tests were carried out using an Autolab PGSTAT302N potentiostat. A typical three-electrode system, with a platinum microelectrode (2 mm diameter) as the working electrode, a platinum disc electrode (5 mm×5 mm) as the counter electrode and an Ag wire as the reference electrode, was used to implement the electrochemical tests. The working electrode and

counter electrode were polished with 0.3 μm alumina paste and cleaned with acetone and deionized water before operating the tests. Unless otherwise stated, all electrochemical tests were performed at 70 $^{\circ}\text{C}$.

2.3 Electrodeposition process

A copper plate (30 mm \times 7 mm) was used as the cathode and a piece of pure Zn plate was used as the anode for the electrodeposition process. Before electrodeposition, the copper plate was polished and activated in a 5 wt% hydrochloric acid for 30 s. All the electrodeposition processes were carried out by a single pulse galvanostatic method with a duty cycle of 50% and pulse frequency of 1000 Hz at a current density of 4 mA cm $^{-2}$ for 120 min. The temperature was kept at 70 $^{\circ}\text{C}$ during electrodeposition with constant agitation (1000 rpm).

2.4 Coating characterization

The surface morphology of the GO sheets, Zn coatings and the distribution of GO sheets were observed using scanning electron microscopy (SEM, JEOL, JSM-5600LV) with energy dispersive spectroscopy (EDS, KeveX). X-ray diffraction (XRD) analysis was performed by a D/MAX-2400 (Rigaku, Japan) with a Cu-K α target ($\lambda=0.15406$ nm) at a scan rate of 5 $^{\circ}$ min $^{-1}$. X-ray photoelectron spectroscopy (XPS) measurements were performed using a ESCALAB 250Xi with a monochromated Al K α radiation (1486.6 eV). Calibration of all XPS spectra was conducted using the C1s line at 284.8 eV and curve fitting and background subtraction were conducted by XPS PEAK Version 4.0 software. The corrosion resistance of the coatings was evaluated by potentiodynamic polarization and electrochemical impedance spectroscopy (EIS) tests using an Autolab PGSTAT302N potentiostat in naturally aerated 3.5% NaCl solution. A three-electrode system, with the coated specimen as working electrode (with 0.25 cm 2 exposure area), a platinum plate as counter electrode and a Ag/AgCl (saturated with KCl) electrode as reference electrode was used. The specimens were immersed in the NaCl solution for about 60 min before potentiodynamic polarization and EIS tests to ascertain stable open

circuit potentials (OCPs). The potentiodynamic polarization was performed from -1.6 V to -0.7 V (referred to the Ag/AgCl electrode) at a scanning rate of 1 mV s $^{-1}$. EIS measurements with an alternating current signal of frequency range from 30 kHz to 10 mHz were conducted at the OCP with an AC amplitude of 10 mV. All the electrochemical tests were carried out at room temperature.

3. Results and Discussion

3.1 The dispersion stability of GO sheets

Fig. 1 shows the SEM images of the GO sheets used as the reinforcements of the Zn-matrix composite coating in this work. It revealed that the thin GO sheets are crumpling and the surface of GO sheets is quite smooth. The dispersion stability of GO sheets in ChCl:2urea DES with 0.2 M ZnCl $_2$ and in deionized water with 0.2 M ZnCl $_2$ was compared under static condition at room temperature and the results are shown in Fig. 2. The GO sheets settle down quickly in deionized water with 0.2 M ZnCl $_2$, though it can be wetted and stable for a long time in pure deionized water. The reason is that the major sorption mechanism of the metal ions and surface functional groups of GO in aqueous solution is chemical interaction. The protons in the functional groups of GO can exchange with metal ions in aqueous solution, resulting in poor dispersion stability.²⁷ However, a stable suspension of GO sheets in the ChCl:2urea DES with 0.2 M ZnCl $_2$ (more than 30 days) is observed. This is due to the ChCl:2urea DES has higher viscosity and ionic strength than that of deionized water, which can effectively decrease the setting velocity of GO sheets and weaken the interaction of GO sheets to prevent the agglomeration process.²⁷ Thus, DES is an ideal dispersion medium of GO. Furthermore, considering the possibility that the Zn(II) cations were adsorbed by GO in the electrolyte and formed the ionic clouds on the GO surface, it can be inferred that the GO particles are positively charged.²⁹

3.2 Effect of GO on the electrochemical behavior of Zn(II) in ChCl:2urea DES

The cyclic voltammetry and potential step experiments were used to investigate the effect of GO on the electrochemical behavior of Zn(II) in ChCl:2urea DES. Cyclic voltammograms (CVs) in ChCl:2urea DES with 0.2 M ZnCl₂ in the absence and presence of GO on a Pt electrode at 70 °C are showed in Fig. 3. The cathodic reaction at ca. -1.05 V associates with the reduction of Zn(II) to Zn. The anodic reaction at ca. -0.85 V is assigned to the oxidation of Zn. It can be seen from the CV curves that the peak currents (*i*_{pc}) for the Zn(II) in DES containing GO are higher than that without GO. Furthermore, the reduction peak potentials positively shift and the peak currents increase with the increase of the GO concentrations in DES. The change of the conductivity of the electrolyte with addition of GO (the conductivities of electrolyte with 0, 0.05 g L⁻¹ and 0.10 g L⁻¹ GO are 13.23 mS/cm, 13.29 mS/cm and 13.34 mS/cm, respectively) is very small, which is not enough to lead to so obvious changes in the reduction current. It can be inferred that the change of CV behavior suggests that GO facilitates the nucleation/growth of Zn in the DES. There are two possible reasons for the facilitation of GO on the nucleation/growth process. Firstly, the part of the unsaturated oxygen atoms on oxygen-containing functional groups of GO can combine with the absorbed zinc atoms and form zinc-oxygen chemical bonds.³⁰ Secondly, the GO sheets act as a hydrogen bond donor to reduce the activity of free chloride ions close to the electrode surface in a certain degree. The decrease of the chloride ions activity will increase the relative concentration of [ZnCl₄]²⁻ close to the electrode surface and thus facilitate the reduction process of Zn.³¹

To elucidate the nucleation/growth process of Zn in ChCl:2urea DES with and without GO, chronoamperometric (CA) experiments were carried out under a series of step potentials and the results are illustrated in Fig. 4a-b. For the DES without GO, the currents sharply drop when the potentials are applied to the electrode as shown in Fig. 4a. Then the currents increase rapidly and reach a maximum current (*i*_m) at a time (*t*_m). After that, the currents decrease slowly and finally flatten out. This is a typical current-time behavior of the diffusion-limited nucleation process.³² It is also

found that the *i*_m increases while the *t*_m shortens with the applied potentials moving to negative values, which means that more negative potential facilitates the nucleation process of Zn. For the DES with 0.10 g L⁻¹ GO, the change trend of current-time curves is similar to that of the DES without GO (Fig. 4b). Under the same applied potential, however, the DES with GO has higher maximum current and shorter *t*_m than that without GO, indicating that GO sheets are conducive to the Zn nucleation/growth process. The results are in agreement with the investigations of the CV tests.

Scharifker-Hills³³ nucleating model is widely used for elucidating the electrocrystallization process. There are two limiting types of the model: three-dimensional (3D) instantaneous nucleation and three-dimensional progressive nucleation. The expressions of instantaneous (Eq. (1)) and progressive (Eq. (2)) nucleation are represented, respectively, by

$$\left(\frac{i}{i_m}\right)^2 = 1.9542\left(\frac{t}{t_m}\right)^{-1} \left\{1 - \exp\left[-1.2564\left(\frac{t}{t_m}\right)\right]\right\}^2 \quad (1)$$

$$\left(\frac{i}{i_m}\right)^2 = 1.2254\left(\frac{t}{t_m}\right)^{-1} \left\{1 - \exp\left[-2.3367\left(\frac{t}{t_m}\right)\right]\right\}^2 \quad (2)$$

Fig. 4c-d shows the non-dimensional *i*²/*i*_m² vs. *t*/*t*_m curves of Zn in the ChCl:2urea DES with and without GO. For the ChCl:2urea DES without GO, the Zn nucleation initially fits most closely to a 3D progressive mechanism and then gradually changes to 3D instantaneous mechanism (Fig. 4c). The Zn nucleation mechanism in ChCl:2urea DES with GO initially follows 3D instantaneous nucleation and then deviates from the theoretical model at longer time scale as shown in Fig. 4d. The difference of Zn nucleation mechanisms can be attributed to the presence of GO in the ChCl:2urea DES changing the thickness of electrical double layer and the surface charge of particles.³⁴

3.3 Microstructure and compositions

Fig. 5 displays the XRD patterns of the coatings deposited from the ChCl:2urea DES containing different concentrations of GO. The XRD pattern of GO sheets used in this work is shown in the inset of Fig. 5. The single peak at 2θ=9.6° is assigned to (001) crystalline plane of GO

(inset in Fig. 5), indicating that the GO sheets have a higher purity. The diffraction peaks of the coating deposited from the DES without GO agree well with the reference patterns for the standard PDF card of Zn (No. JCPDS 65-3358). There are one intensive peak at $2\theta = 43.4^\circ$ and two weak peaks at $2\theta = 38.6^\circ$ and 36.3° , corresponding to the (101), (100) and (002) crystal plane of Zn, respectively. However, different characteristics of the XRD patterns are presented for the coatings deposited from the DES with GO. Except for the Zn diffraction peaks, the diffraction peaks corresponding to GO can also be identified in the pattern, which means that the GO sheets were embedded into the Zn coating. However, the GO peak shifted to lower 2θ values (ac. 8.7°), which is strong evidence of the intercalation of metal ions (Zn^{2+}).³⁵ Furthermore, the presence of GO in the DES changes the preferred crystal orientation of the Zn from (101) to (002) plane and the increase of GO concentration makes the intensity of (002) peak increased while the intensity of (101) and (100) peaks decreased. The change of the preferred orientation of Zn coatings can be attributed to the change of the surface energy differences, which is the driving force for the growth of grains.³ This shows that the (002) plane of Zn in the presence of GO have the lowest surface energy. Therefore, the XRD analysis clearly indicates that Zn-GO composite coatings are successfully electrodeposited from the DES containing GO sheets.

The XPS analysis was performed to further understand the elemental composition and valence of the Zn-GO composite coatings. The C1s spectra of GO, Zn-0.05GO and Zn-0.10GO specimens are shown in Fig. 6a-c, the ratios of carbon to oxygen (C/O) are ca. 1.28, 2.72 and 2.17, respectively. The lower ratio of C/O in GO indicates the high oxidation of the graphene sheets. An increase in the ratios of C/O in Zn composite coatings shows that part oxygen functional groups were removed and the GO was partially reduced during the electrodeposition process.¹⁹ According to the quantitative analysis of the XPS data, the binding energy and corresponding percentage of C species are summarized in Table 1. The C1s spectrum of GO (Fig. 6a) can be deconvoluted into four peaks

centered at 284.50, 285.00, 286.92 and 287.98 eV, which are associated with sp^2 or sp^3 -hybridized carbon (C=C or C-C), C-O, C=O and O=C-O groups, respectively.¹⁹ The C1s spectrum of Zn-GO composite coatings can also be fitted to four peaks corresponding to C=C or C-C, C-O, C=O and O=C-O. Compared with C1s spectrum of GO, the binding energy of the first two C species almost perfectly correlated with each other. However, the binding energy of C=O and O=C-O of Zn-GO composite coatings shifts ca. 1.63 and 1.47 eV to the higher binding energy direction, which may be caused by the interaction of GO and Zn^{2+} , i.e., $\text{C=O} \rightarrow \text{Zn}$.^{14, 20} Compared with the C1s spectrum of GO, the percentage of C=C/C-C and C-O of Zn-GO composite coatings increases markedly. However, the content of C=O and O=C-O of Zn-GO decreases. The results means that partial carbonyl and carboxyl groups had been removed from GO during the electrodeposition process. In addition to the C1s peak, the Zn 2p peaks in pure Zn and Zn-GO composite coatings also have some changes (Fig. 6d). For pure Zn coating, the peaks of Zn 2p_{1/2} and Zn 2p_{3/2} are located at 1021.58 and 1044.68, respectively, but those in Zn-GO composite coatings were shifted to 1021.48, 1044.58 (Zn-0.05GO) and 1021.28, 1044.38 (Zn-0.10GO), respectively. The shifts of peaks position can be attributed to the chemical interaction between Zn and GO.³⁶

SEM micrographs of Zn and Zn-GO composite coatings are presented in Fig. 7. The pure Zn coating was uniform and shows typical polyhedral structure with the grains size of 2-5 μm (Fig. 7a). The Zn-GO composite coatings exhibit an obvious refined grains and the grain shape change from polyhedron to granule (Fig. 7b-c). The grain refinement could be attributed that the GO particles act as effective preferential nucleation sites facilitating the nucleation rate, while decreasing the grow rates of Zn nuclei.²⁵ In addition, some irregularly shaped sheets present and distribute randomly in the coating (Fig. 7b-c). It is sure that these irregular shaped sheets are GO embedded into the Zn coating, which has been identified by above-mentioned XRD and XPS analyses. Further, the EDS mapping of surface morphology and cross-section for the Zn-GO

composite shown in Fig. 8 clearly demonstrated that the elements of C and O corresponding to the GO present in the coatings and their distribution agrees well with that of the sheets in SEM image. It is clear that the number of the sheets increases with the increase of the GO concentration in DES. The positive charged GO particles convected towards the cathode in electric field and entrapped into the Zn matrix with the reduction of the Zn(II) ions, resulting in the embedding of GO into the Zn matrix.

3.4 Electrochemical corrosion behavior

The potentiodynamic polarization curves of the pure Zn and Zn-GO composite coatings with different GO concentrations in naturally aerated 3.5% NaCl solution are presented in Fig. 9. The corrosion potential (E_{corr}) and corrosion current density (i_{corr}) of the specimens were fitted by Tafel extrapolation from the polarization curves and the results are listed in Table 2. It can be seen from Fig. 9 and Table 2 that all Zn-GO composite coatings exhibit more positive E_{corr} and lower i_{corr} than that of the pure Zn coating. Furthermore, the higher GO concentration in the DES, the more positive E_{corr} and lower i_{corr} were measured for the Zn-GO composite coatings. The Zn-0.10GO composite coating has a 131 mV positive shift of E_{corr} and more than two orders of magnitude lower i_{corr} than the pure Zn coating. From the polarization curves, it can be seen that all coatings exhibit passive regions, suggesting that the pure Zn and Zn-GO composite coatings can be passivated in the corrosive solution. However, the passivation current densities of the Zn-GO composite coatings are much lower than that of the pure Zn coating and surprisingly the second passivation are recorded for the Zn-GO composite coatings. The occurrence of the second passivation may be ascribed to the interaction between corrosion products of Zn coating - Zn(II) cations and GO to form a higher stability of Zn/GO composite. It was reported that the oxygen in the GO can interact with metal ions to form a functionalized GO (M/GO).²⁰ However, more detailed investigations need to be done to understand the formation of the Zn/GO composite related to the second passivation.

From the results of polarization tests, it is clear that the Zn-GO composite coatings have better corrosion resistance than the pure Zn coating in 3.5 wt% NaCl solution and the corrosion resistance of Zn-GO composite coatings increased with increasing the GO concentration in DES. Taking into account the structure and composition characteristics of the pure Zn and Zn-GO composite coatings, their corrosion process can be schematically proposed in Fig. 10. For the pure Zn coating, a passive layer was formed in the corrosive solution may be due to the dissolution of naturally formed oxides and the formation of hydroxyl/chloride corrosion products,³⁷ which is corresponding to the first passivation process in Fig. 10. However, the passive layer had some defects (pores and cracks), deteriorating the corrosion resistance of the Zn coating. For the Zn-GO composite coatings, more compact passive layer can be formed in the first passivation process,³⁸ which provided better corrosion resistance than that of pure Zn coating. With the development of the corrosion process, the corrosion products of Zn coating - Zn(II) cations combined with GO to form a higher stability of Zn/GO composite, resulting in the second passivation process. Therefore, the improvement of the corrosion resistance for the Zn-GO composite coating can be ascribed to two aspects. On one hand, the addition of GO in the DES changed the crystal structure and morphology of the Zn coating, resulting in a more compact passive layer and the enhancement of the corrosion resistance. On the other hand, the zinc cations derived from the corrosion of Zn coating could interact with GO to form a Zn/GO composite products, which are probably beneficial for corrosion-resistant performance.

The EIS measurements were implemented to further investigate the corrosion resistance of Zn and Zn-GO composite coatings. The impedance results are exhibited by Nyquist and Bode plots as shown in Fig. 11. It can be clearly seen from Fig. 11a that the Nyquist plots of Zn coating is characterized by a capacitive loop at high frequency region and a capacitive loop at low frequency region. The high frequency capacitance loop is related to the charge transfer resistance and the electric-double layer capacitance.³⁹ The low frequency capacitance loop indicates the presence

of a porous corrosion product layers on the metal surface.⁴⁰ However, the Nyquist plots of Zn-GO composite coatings are characterized by a capacitive loop at high frequency region and followed by a linear component at low frequency region. The high frequency capacitive loop is in accord with the corrosion resistance of Zn coating. The linear at low frequency region is attributed to the diffusion process of reacting chemical species through the coating,⁴¹ indicating that the corrosion process of Zn-GO composite coatings is controlled not only by a charge transfer process, but also by a diffusion process.⁴² This may be ascribed to the GO sheets and Zn/GO composite products act as the geometric blocking layers in Zn-GO composite coatings and therefore affect the diffusion of corrosion ions. However, the linear slope in the Nyquist plots of the composite coatings are less than 45° , suggesting that the formation of porous Zn/GO composite layers. Similar result has been reported by Chen.⁴⁰ From Fig. 11a, it can also be observed that the Zn coating has the smallest diameter of semicircle and the diameter of semicircle of the composite coatings increase with the increase of GO concentration.

The impedance spectra for Nyquist diagram were fitted by the two different equivalent electrical circuit (EEC) models illustrated in Fig. 11a. The validity of these models is confirmed based on the better nonlinear least square fits of the experimental data to within 5% error. In the equivalent circuits, R_s is the solution resistance, R_1 and CPE_1 represents the charge transfer resistance and the double layer capacitance at the electrolyte/coated surface interface, respectively. For the pure Zn coating, the elements of R_2 and CPE_2 represent the resistance of the corrosive ions through the passive layer or corrosion layer and the corresponding capacitance. The elements of R_2 and CPE_2 represent the resistance of the passive layer of Zn-GO composite coatings and the corresponding capacitance. W represents the diffusion of the electroactive species through the Zn composite coating or the corrosion layer. The constant phase element, CPE, is used to instead of a pure double layer capacitor to obtain a more accurate fit due to the distributed surface reactivity, roughness and surface heterogeneity.⁴² The fitted

results of circuit elements are shown in Table 3. From the fitted data, it can be seen that the values of R_1 and R_2 have a significantly increase for the Zn-GO composite coatings compared to pure Zn coating, implying an increase in corrosion resistance of coatings after incorporated GO sheets due to the change of microstructure and the formed of compact passive layer or corrosion product layers. Meanwhile, the values of CPE_1 and CPE_2 decreased greatly for Zn-GO composite coatings. The decreases of CPE_1 suggest that the passivating layer or corrosion layer becoming less permeable. The decline of CPE_2 show that the reduction of active surface area owing to the formation and accumulation of insoluble corrosion products, which directly in contact with the corrosion medium.

From the Bode plots (Fig. 11b and c), it can be seen that both the pure Zn and Zn-GO composite coatings were characterized with two time constant. The value of $|Z|_{f \rightarrow 0}$ in the Bode plot is used to assess the corrosion resistance of the coatings in this work. The higher values of $|Z|_{f \rightarrow 0}$ means that the higher corrosion resistance. The corrosion resistance of the coatings, which is represented by the value of $|Z|_{f=0.01 \text{ Hz}}$ in Fig. 11b, are in agreement with the investigation of the Nyquist plots. Therefore, the results further showed that the Zn-GO composite coatings have a higher corrosion resistance than the Zn coating, and the corrosion resistance of Zn-GO composite coatings increases with the increase of GO concentration

4. Conclusions

In this paper, we develop a GO enhanced Zn matrix composite coatings in $\text{ChCl}:\text{2urea DES}$. The GO sheets not only exhibit excellent dispersion stability in $\text{ChCl}:\text{2urea DES}$ with 0.2 M ZnCl_2 , but also act as preferential nucleation sites facilitating the electrodeposition process. The presence of GO had a significantly influence on the surface morphology and phase structure of Zn coating.

Compared to the pure Zn coating, the Zn-GO composite coatings have better corrosion resistance and the corrosion resistance of Zn-GO composite coatings increase with GO content increasing. This work opens new possibilities for study of DES as a medium for dispersion of GO and electrodeposition of anti-corrosion GO enhanced metal matrix composite coatings.

Acknowledgements

The financial supports from National Natural Science Foundation of China (Grant No. 51305432) and the "Hundred Talents Program" of Chinese Academy of Sciences (J. Liang) were gratefully acknowledged.

References

- 1 B.M. Praveen and T.V. Venkatesha, *Appl. Surf. Sci.*, 2008, **254**, 2418-2424.
- 2 S. Hashimoto and M. Abe, *Corros. Sci.*, 1994, **36**, 2125-2137.
- 3 S. Ranganatha, T.V. Venkatesha, K. Vathsala and M.K. Punith Kumar, *Surf. Coat. Technol.*, 2012, **208**, 64-72.
- 4 B.M. Praveen, T.V. Venkatesha, Y. Arthoba Naik and K. Prashantha, *Surf. Coat. Technol.*, 2007, **201**, 5836-5842.
- 5 M. Sajjadnejad, A. Mozafari, H. Omidvar and M. Javanbakht, *Appl. Surf. Sci.*, 2014, **300**, 1-7.
- 6 M.K. Punith Kumar, M.P. Singh and C.D. Srivastava, *RSC Adv.*, 2015, **5**, 25603-25608.
- 7 S. Ranqanatha and T.V. Venkatesha, *RSC Adv.*, 2014, **4**, 31230-31238.
- 8 C.D. Gu, H. Zhang, X.L. Wang and J.P. Tu, *RSC Adv.*, 2013, **3**, 11807-11815.
- 9 B.P. Singh, B.K. Jena, S. Bhattacharjee and L. Besra, *Surf. Coat. Technol.*, 2013, **232**, 475-481.
- 10 A. Lerf, H.Y. He, M. Forster and J. Klinowski, *J. Phys. Chem. B*, 1998, **102**, 4477-4482.
- 11 S. Stankovich, R.D. Piner, S.T. Nguyen and R.S. Ruoff, *Carbon*, 2006, **44**, 3342-3347.
- 12 T. Szabó, E. Tombácz, E. Illés and I. Dékány, *Carbon*, 2006, **44**, 537-545.
- 13 H.C. Tian, J.Q. Liu, D.X. Wei, X.Y. Kang, C. Zhang, J.C. Du, B. Yang, X. Chen, H.Y. Zhu, Y.N. Nuli and C.S. Yang, *Biomaterials*, 2014, **35**, 2120-2129.
- 14 S.W. Su, B.B. Chen, M. He and B. Hu, *Talanta*, 2014, **123**, 1-9.
- 15 H. Bai, C. Li, X.L. Wang and G. Shi, *Chem. Commun.*, 2010, **46**, 2376-2378.
- 16 X.Y. Yang, X.Y. Zhang, Y.F. Ma, Y. Huang, Y.S. Wang and Y.S. Chen, *J. Mater. Chem.*, 2009, **19**, 2710-2714.
- 17 X.M. Sun, Z. Liu, K. Welscher, J.T. Robinson, A. Goodwin, S. Zaric and H. Dai, *Nano Res.*, 2008, **1**, 203-212.
- 18 M. Li, Q. Liu, Z.J. Jia, X.C. Xu, Y. Cheng, Y.F. Zheng, T.F. Xi and S.C. Wei, *Carbon*, 2014, **67**, 185-197.
- 19 W.T. He, L.Q. Zhu, H.N. Chen, H.Y. Nan, W.P. Li, H.C. Liu and Y. Wang, *Appl. Surf. Sci.*, 2013, **279**, 416-423.
- 20 M. Marimuthu, M. Veerapandian, S. Ramasundaram, S.W. Hong, P. Sudhagar, S. Nagarajan, V. Raman, E. Ito, S. Kim, K. Yun and Y.S. Kang, *Appl. Surf. Sci.*, 2014, **293**, 124-131.
- 21 K. Krishnamoorthy, K. Jeyasubramanian, M. Premanathan, G. Subbiah, H.S. Shin and S.J. Kim, *Carbon*, 2014, **72**, 328-337.
- 22 A.P. Abbott and K.J. McKenzie, *Phys. Chem. Chem. Phys.*, 2006, **8**, 4265-4279.
- 23 A.P. Abbott, K.E. Ttaib, G. Frisch, K.J. McKenzie and K.S. Ryder, *Phys. Chem. Chem. Phys.*, 2009, **11**, 4269-4277.
- 24 R.Q. Li, Q.W. Chu and J. Liang, *RSC Adv.*, 2015, **5**, 44933-44942.
- 25 M. Eslami, H. Saghafian, F. Golestani-fard and A. Robin, *Appl. Surf. Sci.*, 2014, **300**, 129-140.
- 26 Y.H. You, C.D. Gu, X.L. Wang and J.P. Tu, *Int. J. Electrochem. Sci.*, 2012, **7**, 12440-12455.
- 27 P. Martis, V.S. Dilimon, J. Delhalle and Z. Mekhalif, *Electrochim. Acta*, 2010, **55**, 5407-5410.
- 28 X.B. Yan, J.T. Chen, J. Yang, Q.J. Xue and P. Miele, *ACS Appl. Mat. Interfaces*, 2010, **2**, 2521-2529.
- 29 C.T.J. Low, R.G.A. Wills and F.C. Walsh, *Surf. Coat. Technol.*, 2006, **201**, 371-383.

- 30 W.Y. Tu, B.S. Xu, S.Y. Dong, H.D. Wang and J. Bin, *J. Mater. Sci.*, 2008, **43**, 1102-1108.
- 31 A.P. Abbott, J.C. Barron, G. Frisch, K.S. Ryder and A.F. Silva, *Electrochim. Acta*, 2011, **56**, 5272-5279.
- 32 H.Y. Yang, X.W. Guo, X.B. Chen, S.H. Wang, G.H. Wu, W.J. Ding and N. Birbilis, *Electrochim. Acta*, 2012, **63**, 131-138.
- 33 B. Scharifker and G. Hills, *Electrochim. Acta*, 1983, **28**, 879-889.
- 34 A.P. Abbott, J.C. Barron, G. Frisch, S. Gurman, K.S. Ryder and A. Fernando Silva, *Phys. Chem. Chem. Phys.*, 2011, **13**, 10224-10231.
- 35 S.J. Park, K.S. Lee, G. Bozoklu, W.W. Cai, S.T. Nguyen and R.S. Ruoff, *ACS Nano*, 2008, **2**, 572-578.
- 36 H.N. Tien, V.H. Luan, L.T. Hoa, N.T. Khoa, S.H. Hahn, J.S. Chung, E.W. Shin and S.H. Hur, *Chem. Eng. J.*, 2013, **229**, 126-133.
- 37 M.C. Li, L.L. Jiang, W.Q. Zhang, Y.H. Qian, S.Z. Luo and J.N. Shen, *J. Solid State Chem.*, 2007, **11**, 1319-1325.
- 38 C. Cachet, F. Ganne, S. Joiret, G. Maurin, J. Petitjean, V. Vivier and R. Wiart, *Electrochim. Acta*, 2002, **47**, 3409-3422.
- 39 V. Barranco, S. Feliu Jr and S. Feliu, *Corros. Sci.*, 2004, **46**, 2203-2220.
- 40 Y. Chen and W.P. Jepson, *Electrochim. Acta*, 1999, **44**, 4453-4464.
- 41 Y. Chen, T. Hong, M. Gopal and W.P. Jepson, *Corros. Sci.*, 2000, **42**, 979-990.
- 42 P. Baghery, M. Farzam, A.B. Mousavi and M. Hosseini, *Surf. Coat. Technol.*, 2010, **204**, 3804-3810.

Figure Captions

Fig. 1. SEM images of GO sheets.

Fig. 2. The dispersion stability of GO (0.10 g L^{-1}) in (1) deionized water with $0.2 \text{ mol L}^{-1} \text{ ZnCl}_2$ and (2) ChCl:2urea DES with $0.2 \text{ mol L}^{-1} \text{ ZnCl}_2$.

Fig. 3. Cyclic voltammograms of Zn(II) on Pt electrode in ChCl:2urea containing $0.2 \text{ mol L}^{-1} \text{ ZnCl}_2$ with and without GO sheets (scan rate 50 mV s^{-1}).

Fig. 4. Current-time transients experiments were performed at a Pt electrode in ChCl:2urea DES containing $0.2 \text{ mol L}^{-1} \text{ ZnCl}_2$ by stepping the potential: (a) without GO and (b) with 0.10 g L^{-1} GO. Non-dimensional i^2/i_m^2 vs. t/t_m plots: (c) without GO and (d) with 0.10 g L^{-1} GO.

Fig. 5. XRD patterns of pure Zn and Zn-GO composite coatings. (Inset is the XRD pattern of GO used in this work).

Fig. 6. The C1s XPS spectra of (a) GO, (b) Zn-0.05GO, (c) Zn-0.10GO and (d) the Zn 2p XPS spectrum.

Fig. 7. Surface SEM morphologies of the Zn coatings: (a) without GO, (b) with 0.05 g L^{-1} GO and (c) with 0.10 g L^{-1} GO.

Fig. 8. EDS maps of surface morphology and cross-section for Zn-0.10GO composite coatings.

Fig. 9. Potentiodynamic polarization curves of the pure Zn coating and Zn-GO composite coating in naturally aerated 3.5 wt% NaCl solution.

Fig. 10. Schematic diagrams of the corrosion process of pure Zn and Zn-GO composite coatings.

Fig. 11. Experimental and fitting results of (a) Nyquist and (b, c) Bode plots for pure Zn and Zn-GO composite coatings in naturally aerated 3.5 wt% NaCl solution. Inset: Equivalent circuit for fitting the EIS plots of the Pure Zn coating and the Zn-GO composite coatings.

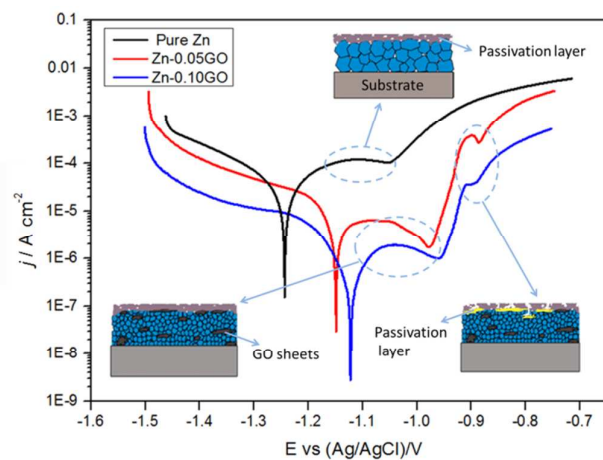
Table List

Table 1 The binding energy and percentage of different C species.

Table 2 Electrochemical data of the pure Zn and Zn-GO composite coatings derived from the polarization tests in naturally aerated 3.5 wt% NaCl solution.

Table 3 EIS fitting results of the specimens in naturally aerated 3.5 wt% NaCl solution.

Graphical Abstract



- The corrosion resistance of Zn-GO is much better than that of pure Zn.

Fig. 1

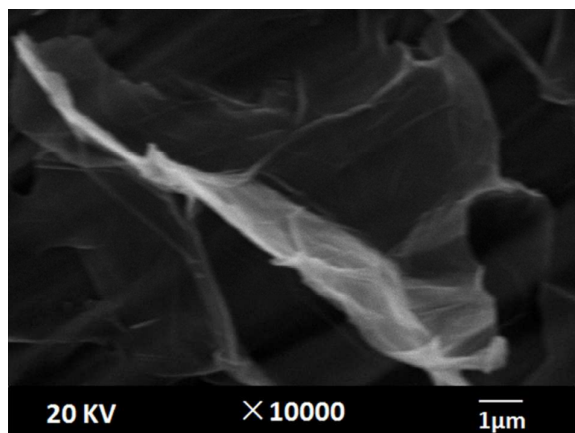


Fig. 2



Fig.3

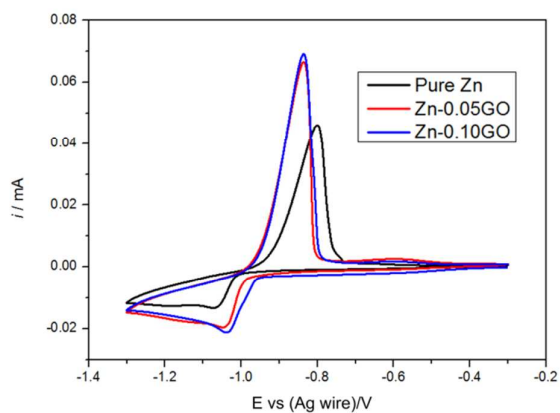


Fig.4.

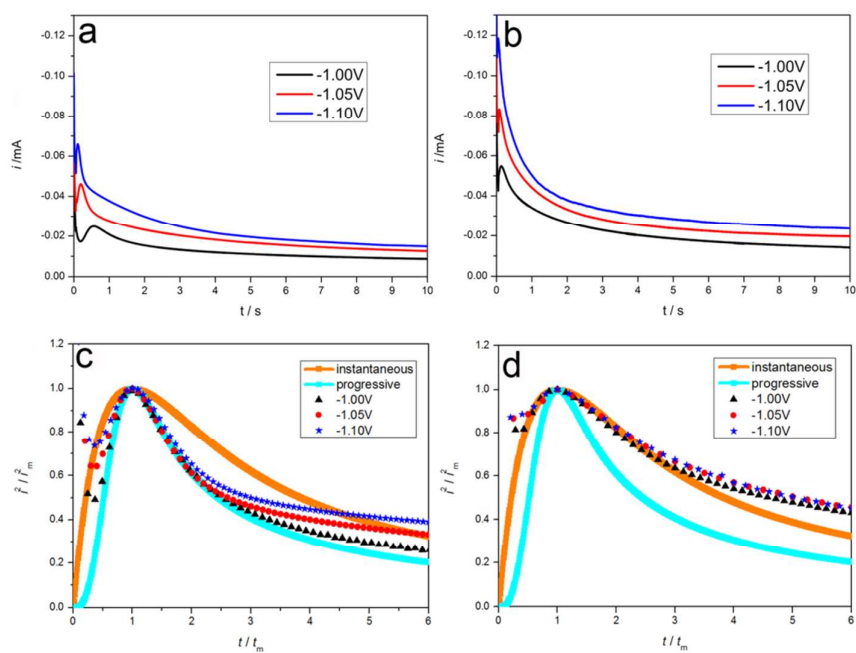


Fig. 5.

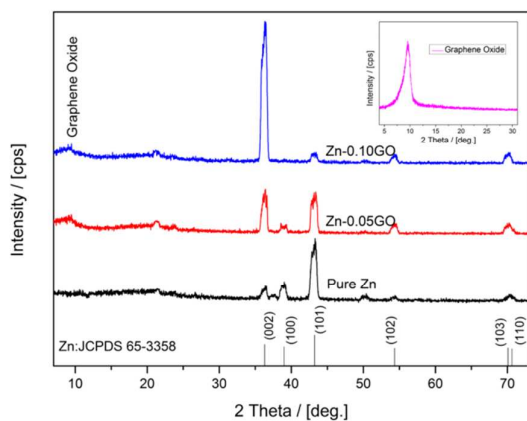


Fig. 6.

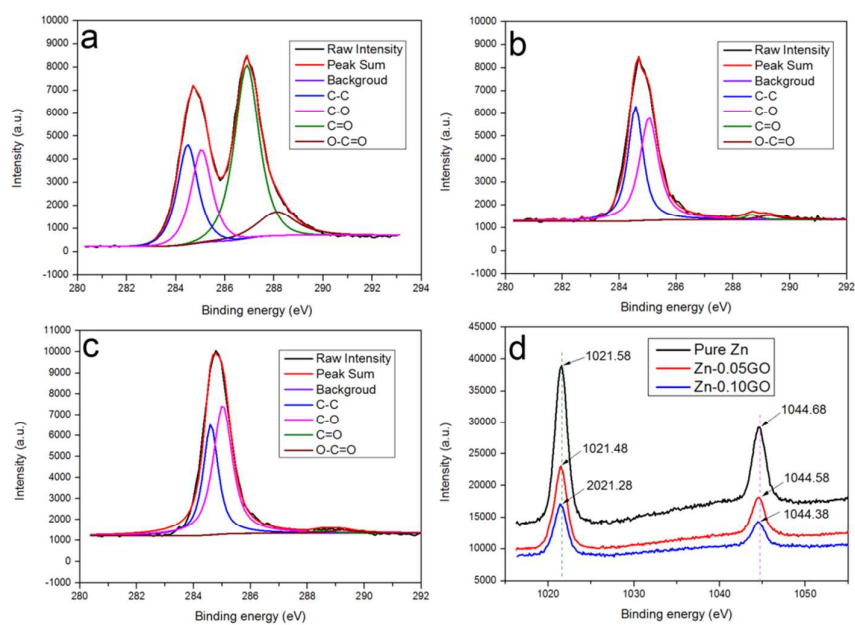


Fig.7.

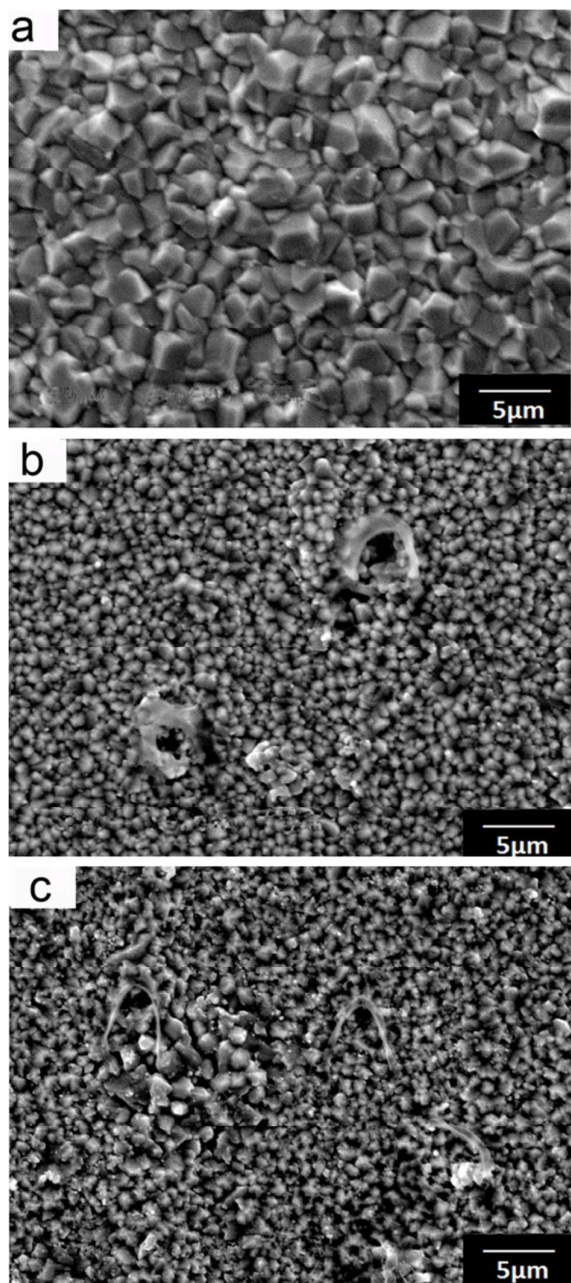


Fig. 8.

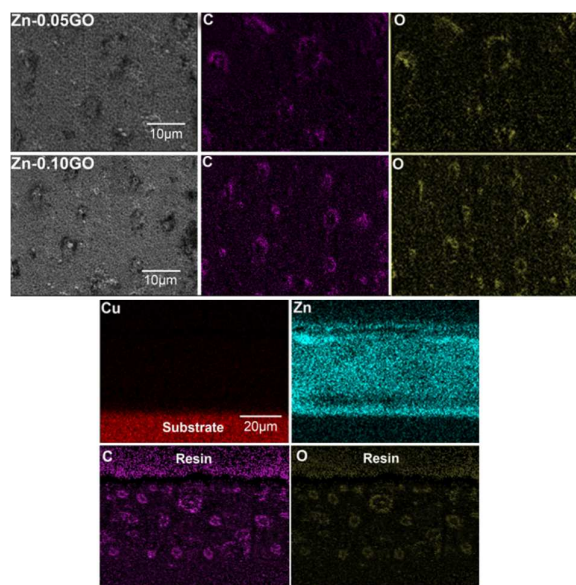


Fig. 9.

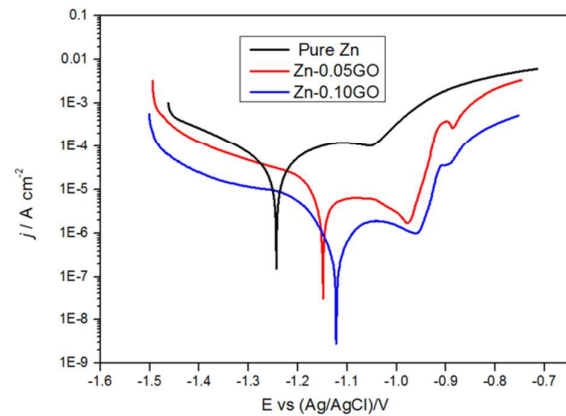


Fig.10.

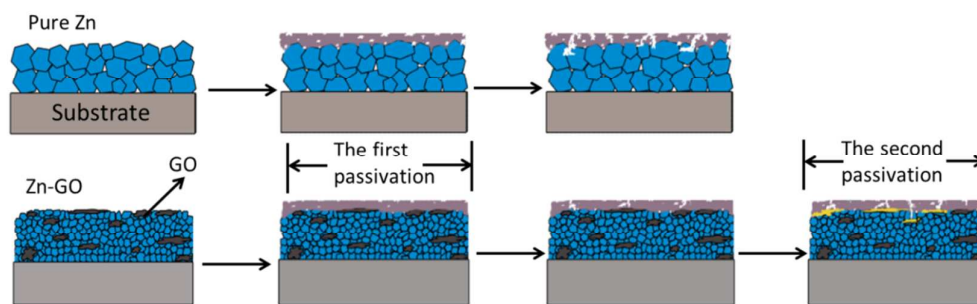
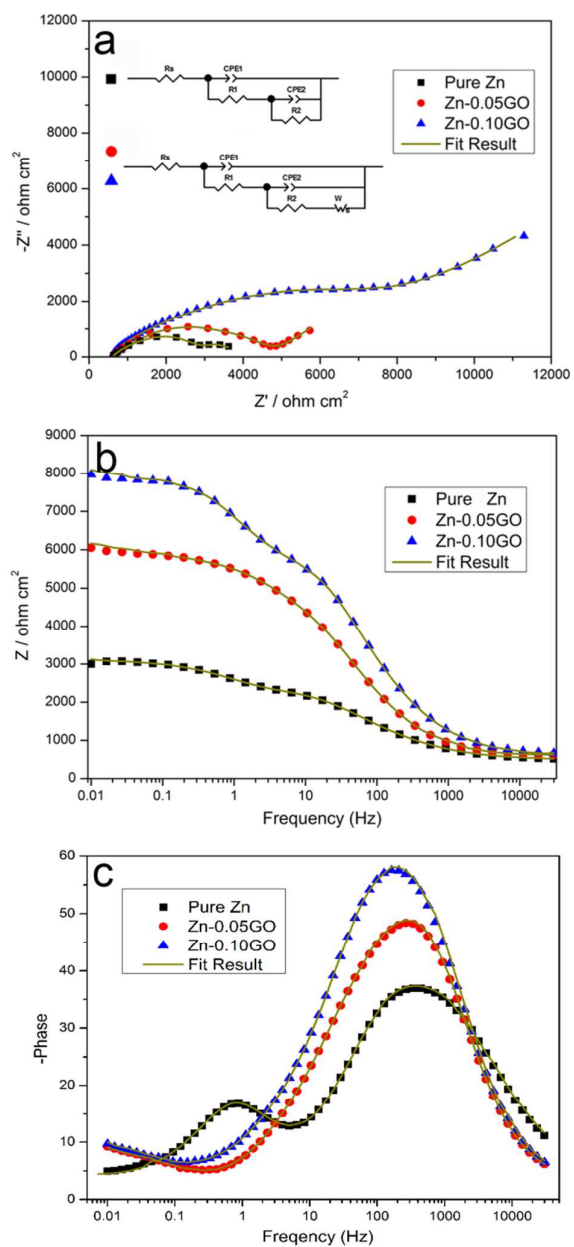


Fig. 11.





ARTICLE

Table 1

	GO		Zn-0.05GO		Zn-0.10GO	
	B.E(eV)	%	B.E(eV)	%	B.E(eV)	%
C-C	284.50	19.8	284.51	39.0	284.57	46.2
C-O	285.00	21.7	285.02	57.5	285.04	49.5
C=O	286.92	46.1	288.55	1.14	288.65	1.67
O-C=O	287.98	12.4	289.23	2.36	289.25	2.63

Table 2

specimens	E_{corr} (V vs. Ag/AgCl)	i_{corr} (A cm^{-2})
Pure Zn	-1.257	6.157×10^{-5}
Zn-0.05GO	-1.151	2.713×10^{-6}
Zn-0.10GO	-1.126	4.812×10^{-7}

Table 3

	R_s	CPE ₁		R_1	CPE ₂		R_2	W
	(Ωcm^2)	$(Y_0)_1$ ($\text{S cm}^{-2} \text{s}^n$)	n_1	($\text{k}\Omega\text{cm}^2$)	$(Y_0)_2$ ($\text{S cm}^{-2} \text{s}^n$)	n_2	($\text{k}\Omega\text{cm}^2$)	(Y_0) ($\text{S cm}^{-2} \text{s}^{1/2}$)
Pure Zn	70.3	4.37×10^{-5}	0.614	0.282	7.5×10^{-4}	0.491	0.427	–
Zn-0.05GO	71.0	4.72×10^{-6}	0.793	0.825	2.09×10^{-5}	0.633	1.281	834
Zn-0.10GO	71.2	1.05×10^{-8}	0.831	1.474	1.57×10^{-6}	0.694	3.202	1138